Nanoparticle Functionalization

DOI: 10.1002/anie.200907032

# Self-Controlled Monofunctionalization of Quantum Dots for Multiplexed Protein Tracking in Live Cells**

*Changjiang You, Stephan Wilmes, Oliver Beutel, Sara Löchte, Yulia Podoplelowa, Friedrich Roder, Christian Richter, Thomas Seine, Dirk Schaible, Gilles Uzé, Samuel Clarke, Fabien Pinaud, Maxime Dahan, and Jacob Piehler**

Tracking the motion of individual proteins on the surface of live cells has contributed considerably towards unveiling the functional organization of proteins in the plasma membrane.[1] Individual proteins labeled with quantum dots (QDs) can be imaged over long time periods with ultrahigh spatial and temporal resolution, yielding powerful information on the spatiotemporal dynamics of proteins at the plasma membrane in live cells.[2–7] A key challenge for the application of QDs is to site-specifically attach proteins to the surface of these nanoparticles in a stoichiometric manner without affecting protein function. Several procedures for rendering surfaces of QDs biocompatible have been described,[4,7–12] thus reducing non-specific binding and protein denaturation on the QD surface. However, functionalized biocompatible QDs used to target cell surface proteins generally result in multipoint attachment to the target proteins because the number of functional groups on the QDs is very difficult to control. Such multiply functionalized QDs induce clustering of target proteins on the cell surface, biasing not only lateral diffusion but also the functional properties of these proteins. As a consequence, increased endocytosis has been observed upon binding of QDs functionalized with multiple epidermal grow factor (EGF) molecules to cell-surface EGF receptors.[3] Stochastic functionalization of multiple reactive sites on the QD offers the choice of obtaining only a minor fraction of the QDs with a single functional group,[3,13] or a significant fraction of QDs with multiple functional groups. Preparation of homogeneous, monofunctional QDs currently relies on electrophoretic purification, which has been achieved only for very small QDs. These compact QDs are designed with very thin surface coatings,[14] which have the disadvantage of showing relatively strong non-specific interactions.

Most approaches for targeting proteins using QDs in live cells are based on biotin–streptavidin interactions, which form quasi-irreversible complexes. For multiplexed, generic labeling of proteins on the cell surface, further targeting strategies are required. We have recently described tris(hydroxymethyl)methylamine–nitrilotriacetic acid (Tris-NTA) moieties for highly specific and stable attachment of fluorophores and other functional units to histidine-tagged proteins in vitro and on the surface of live cells.[15–17] The lifetime of Tris-NTA complexes with His-tagged proteins is in the order of several hours, which is well-suited to medium-term single molecule tracking applications. Herein, we have attempted to control the functionalization degree of QDs with Tris-NTA by means of electrostatic repulsion. We devised a bottom-up coupling chemistry based on a novel Tris-NTA derivative (**1**; Figure 1a), which comprises a thiol-terminated hepta(ethylene glycol) linker. This compound was generated in situ by reduction of the disulfide-linked dimer (**1a**; see the Supporting Information, Scheme S1) and coupled to commercially available polymer-coated and amine-functionalized QDs by means of a hetero-bifunctional cross-linker (Figure 1b). Covalently attachment of **1** to surfaces modified with maleimide-functionalized polyethylene glycol (PEG) polymer brush and specific immobilization of His-tagged proteins was confirmed by label-free detection (Supporting Information, Figure S1). To control the degree of functionalization with Tris-NTA on the QD surface, the reaction of **1** with surface maleimide groups was performed at low ionic strength. Under these conditions, all QDs were reacted with Tris-NTA, as confirmed by an increase in negative charges detected by anion exchange chromatography and agarose gel electrophoreses (Figure 1c,d). These assays indicated relatively monodisperse electrostatic properties after coupling of **1**, despite the fact that it was reacted at a large excess (660 μM of compound **1** to 1 μM QD). Coupling of **1** at higher ionic strength yielded QDs with a substantially higher degree of functionalization, as confirmed by a further shift of the signals both in anion exchange chromatography and agarose gel electrophoresis (Figure 1c,d).

To characterize the functional properties of Tris-NTA-coupled QDs, binding to immobilized hexahistidine (H6)

[*] Dr. C. You, S. Wilmes, O. Beutel, S. Löchte, Y. Podoplelowa, F. Roder, C. Richter, T. Seine, D. Schaible, Prof. Dr. J. Piehler
Division of Biophysics, Universität Osnabrück
Barbarastrasse 11, 49076 Osnabrück (Germany)
Fax: (+49) 541-969-2262
E-mail: piehler@uos.de
Homepage: http://www.biologie.uni-osnabrueck.de/Biophysik/Piehler/

Dr. G. Uzé
CNRS UMR 5124, University Montpellier II
Place Eugène Bataillon, Montpellier (France)

Dr. S. Clarke, Dr. F. Pinaud, Dr. M. Dahan
Département de Physique et de Biologie
Ecole Normale Supérieure, Paris (France)

[**] We thank Gabriele Hikade and Hella Kenneweg for recombinant protein production, and Covalys Biosciences for technical support with PPT labeling. This project was supported by the DFG (PI405-4, PI405-5, and EXC 115), by the Human Frontier Program Organization (RGP 5/2007), and by the EU (FP7, IFNaction).

Supporting information for this article is available on the WWW under http://dx.doi.org/10.1002/anie.200907032.

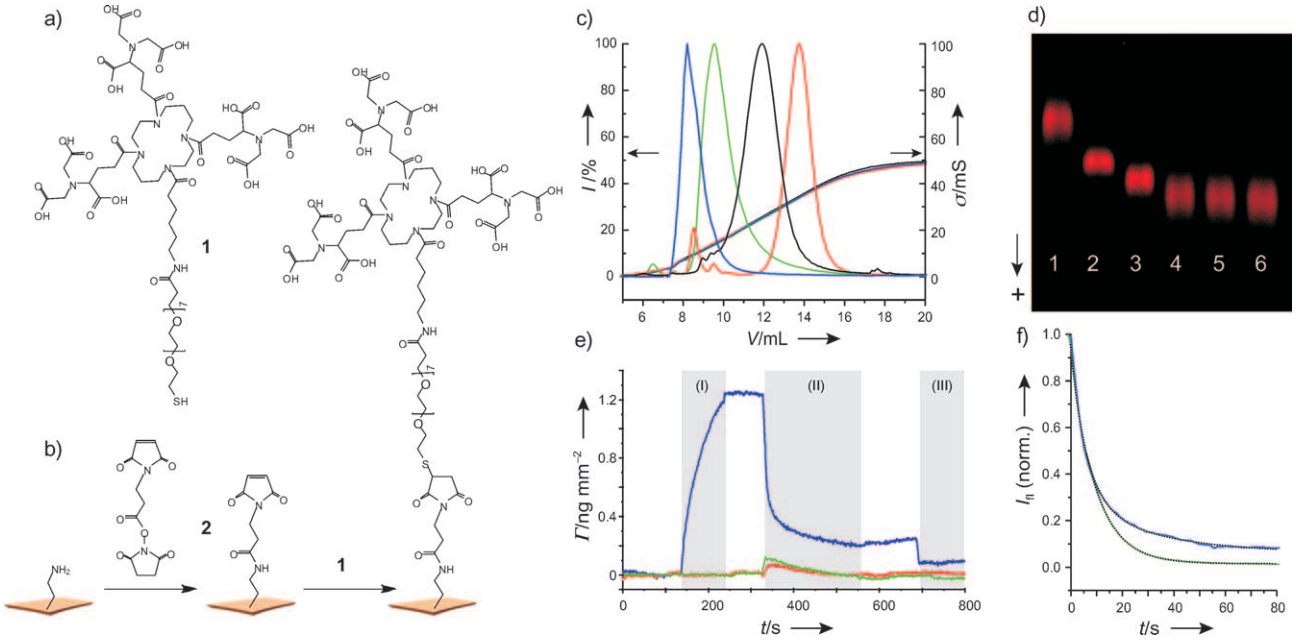


***Figure 1.*** Characterization of Tris-NTA-functionalized QDs in vitro. a) Structure of the Tris-NTA derivative **1** used for surface functionalization. b) Surface amines were treated with 3-maleimidopropionic acid-*N*-hydroxysuccinimidyl ester (MPA-NHS; **2**), and then Tris-NTA-$EG_7$-thiol **1** was coupled. c) Fractionation by anion-exchange chromatography: elution profiles (left *y* axis) and conductivity (right *y* axis) of amine-functionalized QDs (blue), after reaction with MPA-NHS (green), and coupling of **1** at low (black) and high (red) ionic strength. d) Agarose gel electrophoreses of QD before functionalization (lane 1), after reaction with MPA-NHS (2), and after coupling of Tris-NTA at different NaCl concentrations: 3) 0 mM, 4) 150 mM, 5) 400 mM, 6) 1 M. e) Binding of nickel(II)-loaded $^{QD655}$Tris-NTA to a H6 peptide surface and elution with 250 mM imidazole (blue) compared to unmodified QD655 (red) and $^{QD655}$Tris-NTA incubated with 1 mM EDTA (green). I) Injection of QDs, II) elution with 250 mM imidazole, III) regeneration with 100 mM HCl. f) Comparison of the dissociation kinetics for $^{QD655}$Tris-NTA (blue) and $^{OG488}$Tris-NTA (green) from immobilized H6 peptide in the presence of 125 mM imidazole.

peptides was probed by simultaneous total-internal-reflection fluorescence spectroscopy and reflectance–interference (TIRFS-RIF) detection. Fully specific binding was observed only after loading the NTA groups with nickel(II) ions (Figure 1e), thus confirming successful functionalization and selective capturing of His tags by the Tris-NTA moiety. Selective elution with the His-tag competitor imidazole confirmed nickel(II)-mediated binding. We could not detect binding of QDs without Tris-NTA, corroborating efficient shielding of the ZnS surface, which can non-reversibly interact with His-tagged proteins.[18] Upon elution with imidazole, very similar dissociation kinetics compared to Oregon Green 488-labeled Tris-NTA ($^{OG488}$Tris-NTA) was observed (Figure 1f; $k_d = 0.073\ s^{-1}$ and $0.10\ s^{-1}$ for $^{QD655}$Tris-NTA and $^{OG488}$Tris-NTA, respectively), confirming a low degree of Tris-NTA functionalization in the case of coupling at low ionic strength.

Specific protein binding to $^{QD655}$Tris-NTA was explored by analytical size-exclusion chromatography (SEC). For this purpose, nickel(II)-loaded $^{QD655}$Tris-NTA (10 nM) were incubated with a large excess (1 μM) of His-tagged maltose-binding protein (MBP-H10) labeled with a Cy5 analogue dye ($^{FEW646}$MBP-H10). QD-bound $^{FEW646}$MBP-H10 was separated from the free protein by SEC using spectral detection for photometric quantification of $^{QD655}$Tris-NTA and $^{FEW646}$MBP-H10 (Supporting Information, Figure S2). These assays confirmed specific nickel(II)-mediated binding of His-tagged protein to the QD surface. The protein/QD ratio was estimated from the signals at 350 nm ($^{QD655}$Tris-NTA) and 650 nm ($^{QD655}$Tris-NTA + $^{FEW646}$MBP-H10). From these measurements, a protein/QD ratio of 0.9:1 was determined, suggesting an average degree of functionalization of about unity. In conjunction with the observation that all QDs were reacted with Tris-NTA (quantitative shift in anion-exchange chromatography), this result strongly points towards a monodisperse 1:1 functionalization. This observation suggests that electrostatic repulsion may steer the reaction: once a nanoparticle is conjugated with the first Tris-NTA molecule, its highly negative electrostatic potential (six negative charges) efficiently shields coupling of a second Tris-NTA. This effect is maximized by using very low ionic strength and by keeping the NTA moieties free of transition metal ions.

The functional properties of proteins captured to QDs were explored by quantitative protein–protein interaction analysis. For this purpose, we produced Interferon-α2 (IFNα2) fused to an N-terminal decahistidine tag (H10-IFNα2). Nickel(II)-loaded $^{QD655}$Tris-NTA was incubated with a large excess of H10-IFNα2, followed by purification of the $^{QD655}$Tris-NTA/H10-IFNα2 complex by SEC. Binding of $^{QD655}$Tris-NTA/H10-IFNα2 to the extracellular domain of its receptor subunit IFNAR2 (IFNAR2-EC) tethered to solid-supported membranes through a C-terminal H10-tag (Figure 2a) was probed by TIRFS-RIF (Figure 2b). Specific binding to the membrane-bound IFNAR2-EC was observed

  

(Figure 2c), followed by dissociation from the surface during elution with imidazole. The dissociation rate constant $k_d = 0.028 \pm 0.003\ s^{-1}$ determined from the binding curve is only slightly higher than the dissociation rate constant observed for non-labeled IFNα2 ($0.015\ s^{-1}$) and the dissociation rate constant of H10-IFNα2 labeled with $^{OG488}$Tris-NTA ($0.018 \pm 0.002\ s^{-1}$; Supporting Information, Figure S3). In a control experiment, the dissociation rate constant of IFNAR2-EC from H10-IFNα2 immobilized on a PEG polymer brush was determined by TIRFS detection (Supporting Information, Figure S3), yielding a very similar dissociation rate constant ($0.031 \pm 0.001\ s^{-1}$) as that obtained for $^{QD655}$Tris-NTA/H10-IFNα2 binding to immobilized IFNAR2-H10. Importantly, the unbiased dissociation kinetics confirmed the monovalent functionalization of the QDs with Tris-NTA: for multivalent QDs obtained by Tris-NTA coupling at high ionic strength, no ligand dissociation from the surface was observed, as expected for multiple IFNα2 molecules bound to the QD (Supporting Information, Figure S3).

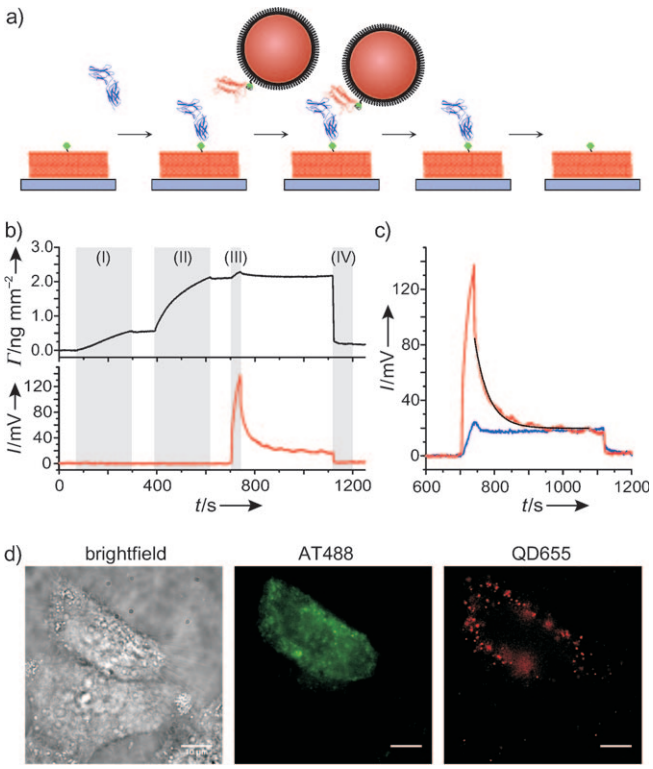


***Figure 2.*** Site-specific protein labeling with $^{QD655}$Tris-NTA. a) Tethering of IFNAR2-EC (blue) onto a solid-supported membrane, binding and dissociation of $^{QD655}$Tris-NTA/H10-IFNα2 (red), and regeneration with imidazole. b) Binding of $^{QD655}$Tris-NTA/H10-IFNα2 to IFNAR2-EC tethered on solid-supported membranes as detected by simultaneous RIF (top) and TIRFS detection (bottom). Gray bars: injection periods for IFNAR2-EC (I), MBP-H10 (II), $^{QD655}$Tris-NTA/H10-IFNα2 (III), and imidazole (IV). c) Binding kinetics of $^{QD655}$Tris-NTA/H10-IFNα2. As a negative control, binding of $^{QD655}$Tris-NTA without H10-IFNα2 to IFNAR2-EC tethered membranes was measured (blue). d) Specific binding of $^{QD655}$Tris-NTA/H10-IFNα2 to HeLa cells expressing IFNAR2-ΔIC. Strong binding of $^{AT488}$IFNα2 to the same cell is shown for comparison. Scale bars: 10 μm.

In the next step, we explored binding of IFNα2 labeled with $^{QD655}$Tris-NTA to IFNAR2 in live cells. For this purpose, HeLa cells were transfected with a plasmid coding for IFNAR2, which was truncated after the transmembrane domain (IFNAR2-ΔIC).[16] Specific binding of IFNα2 labeled with ATTO 488 ($^{AT488}$IFNα2) only to cells overexpressing of IFNAR2-ΔIC at the cell surface was used to detect transfected cells (Figure 2d). Upon incubation of $^{QD655}$Tris-NTA/H10-IFNα2, binding only to the cells expressing IFNAR2-ΔIC was observed, confirming specific ligand binding. High mobility of $^{QD655}$Tris-NTA/IFNα2 on the cell surface was observed by single-molecule tracking. We analyzed the diffusion by single molecule tracking for both $^{AT488}$IFNα2 and $^{QD655}$Tris-NTA/IFNα2 bound to IFNAR2-ΔIC (Supporting Information, Figure S4). From the mean-square displacement (MSD) analysis, diffusion constants of $0.10 \pm 0.02\ \mu m^2 s^{-1}$ and $0.066 \pm 0.003\ \mu m^2 s^{-1}$ were obtained for the mobile fraction of $^{AT488}$IFNα2 and $^{QD655}$Tris-NTA/IFNα2, respectively ($52 \pm 10\%$ and $46 \pm 2\%$, respectively, of all tracked particles).

We have previously demonstrated the high selectivity of Tris-NTA enabling for targeting fluorescence probes to proteins on the cell surface.[15,16] We therefore explored direct labeling of a His-tagged protein on the cell surface with $^{QD655}$Tris-NTA. For this purpose, membrane-anchored CFP fused to an N-terminal H10-tag (H10-CFP-TMD) was expressed in HeLa cells and incubated with nickel(II)-loaded $^{QD655}$Tris-NTA (Figure 3a). Binding of $^{QD655}$Tris-NTA to the cell surface correlated very well with the cell surface expression level of H10-CFP-TMD as detected in the CFP channel. $^{QD655}$Tris-NTA was quantitatively removed from the cell surface by washing with imidazole (Supporting Information, Figure S5), confirming nickel(II)-NTA-mediated binding to the cell surface. High mobility of QDs bound to H10-CFP-TMD was observed (Supporting Information, Figure S6).

The diffusion constant and the mobile fraction determined by single molecule tracking was $0.095 \pm 0.005\ \mu m^2 s^{-1}$ and $49 \pm 2\%$, respectively, corresponding well to the parameters obtained by FRAP ($0.10 \pm 0.02\ \mu m^2 s^{-1}$ and $52 \pm 1\%$; Supporting Information, Figure S6). This finding corroborates wwith unbiased individual protein labeling with $^{QD}$Tris-NTA on the cell surface. With these tools in hand, we combined targeting of cell surface protein and functional labeling of protein in vitro into a dual-color experiment. For this purpose, full-length IFNAR2 fused to an N-terminal H10 (H10-IFNAR2) was first directly labeled with $^{QD525}$Tris-NTA, followed by binding of $^{QD655}$Tris-NTA/IFNα2. Staining with $^{QD525}$Tris-NTA was only observed for cells, which also showed binding of $^{QD655}$Tris-NTA/IFNα2, confirming labeling specificity. No stable co-localization of $^{QD655}$Tris-NTA and $^{QD525}$Tris-NTA was observed, which may be ascribed to the fact that only a small fraction of IFNAR2 on the surface was labeled with QDs (< 5%), resulting into a very low probability for co-localization. This experiment enables to analyze and compare diffusion of IFNAR2 with and without ligand in the same cell.

  

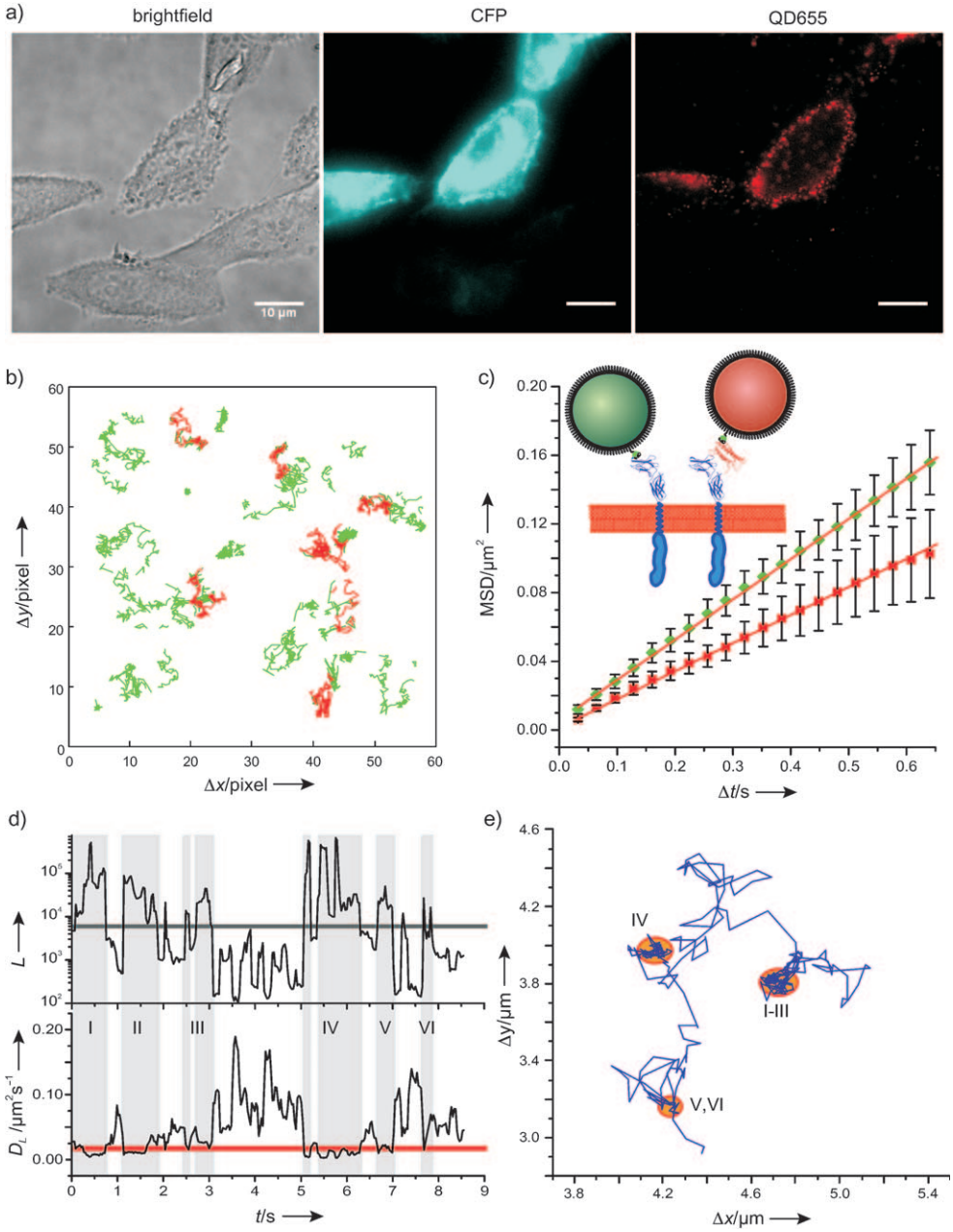


***Figure 3.*** [QD]Tris-NTA-labeled IFNα2 binding and tracking in live cells. a) Comparison of a brightfield image and fluorescence images (CFP and QD655 channels) of cells transiently transfected with H10-CFP-TMD and incubated with nickel(II)-loaded [QD655]Tris-NTA. Scale bars: 10 μm. b) Trajectories obtained for simultaneous tracking of H10-IFNAR2 in live cells labeled with [QD525]Tris-NTA (green) and [QD655]Tris-NTA/H10-IFNα2 (red). c) MSD analysis of [QD525]Tris-NTA/H10-IFNAR2 and [QD655]Tris-NTA/H10-IFNα2 in live cells. d) Analysis of a single trajectory obtained for [QD655]Tris-NTA/H10-IFNα2 showing the local diffusion constant ($D_L$, bottom) and the confinement factor $L$ (top) using an evaluation window of five frames. Sections of the trajectory identified as confined diffusion are highlighted in gray. e) Same trajectory with the confined regions indicated in orange.

Single-molecule tracking of [QD655]Tris-NTA and [QD525]Tris-NTA, and standard MSD analysis, yielded diffusion constants of $0.038 \pm 0.003\ \mu m^2 s^{-1}$ for the IFNα2-IFNAR2 complex and $0.058 \pm 0.002\ \mu m^2 s^{-1}$ for free IFNAR2 alone (Figure 3b,c). Slower diffusion of ligand-bound IFNAR2 may be ascribed to ternary complex formation with endogenous IFNAR1, which is present at relatively low level (ca. 200 receptors/cell).

In vitro binding studies with IFNAR1-H10 and IFNAR2-H10 tethered onto solid-supported membranes confirmed that ternary complex formation upon [QD655]Tris-NTA/IFNα2 binding was possible (Supporting Information, Figure S7). Single-trajectory analysis of the [QD655]Tris-NTA-labeled IFNα2-IFNAR2 complex with respect to local confinement[19] revealed, however, periods of relatively fast diffusion (ca. $0.1\ \mu m^2 s^{-1}$) alternating with periods during which very little mobility can be observed (Figure 3d,e and the Supporting Information). The exact reasons for this behavior need to be explored in the future. Similar events have been previously described, for example, for the EGFR receptor.[19]

In summary, we have demonstrated successful monofunctionalization of QDs with Tris-NTA for selectively capturing His-tagged proteins in vitro and in live cells with a well controlled 1:1 stoichiometry. Our results confirm that electrostatic steering controls nanoparticle functionalization to a 1:1 ratio, in contrast to the Poisson distribution obtained by standard functionalization techniques. Monovalent Tris-NTA QDs have versatile applications for cell surface labeling for unbiased single-molecule tracking: they can not only be directly targeted to His-tagged proteins on the cell surface, but they can also be readily conjugated with any other His-tagged recognition unit, such as monovalent streptavidin[20] or recombinant single-chain antibody fragments in a stoichiometric manner. Indeed, we could also conjugate His-tagged monovalent streptavidin with [QD655]Tris-NTAs for live-cell labeling and tracking of IFNAR1, which

  

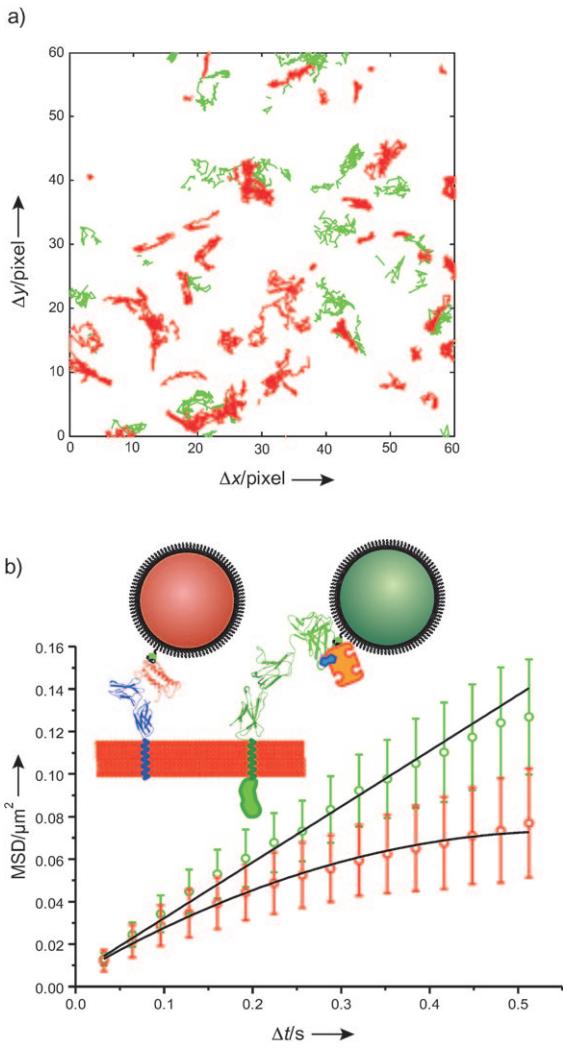


***Figure 4.*** Simultaneous tracking of H10-IFNα2/$^{QD655}$Tris-NTA bound to cell-surface IFNAR2-ΔIC and H6-mSAv/$^{QD525}$Tris-NTA targeted to biotinylated AP-IFNAR1. a) Trajectories obtained for H6-mSAv/$^{QD525}$Tris-NTA/AP-IFNAR1 (green) and for $^{QD655}$Tris-NTA/H10-IFNα2 (red). Image dimensions: 10.8 μm × 10.8 μm. b) Mean-square displacement analysis of H6-mSAv/$^{QD525}$Tris-NTA bound to AP-IFNAR1 (green) and $^{QD655}$Tris-NTA/H10-IFNα2 (red) in live cells. A diffusion constant of $0.066 \pm 0.001\ \mu m^2 s^{-1}$ and a mobile fraction of $32 \pm 3\%$ were obtained for IFNAR1 (green), whilst anomalous diffusion was observed for $^{QD655}$Tris-NTA/H10-IFNα2 (red).

was site-specifically biotinylated through an N-terminal AP tag (Figure 4). Our approach is compatible with most coatings, including those that are commercially available, and should thus provide generic access to monovalent nanoparticle biofunctionalization.

Received: December 14, 2009
Revised: February 10, 2010
Published online: April 29, 2010

**Keywords:** fluorescence microscopy · nanoparticles · protein–protein interactions · quantum dots · receptors

[1] D. Marguet, P. F. Lenne, H. Rigneault, H. T. He, *EMBO J.* **2006**, *25*, 3446.
[2] M. Dahan, S. Levi, C. Luccardini, P. Rostaing, B. Riveau, A. Triller, *Science* **2003**, *302*, 442.
[3] D. S. Lidke, P. Nagy, R. Heintzmann, D. J. Arndt-Jovin, J. N. Post, H. E. Grecco, E. A. Jares-Erijman, T. M. Jovin, *Nat. Biotechnol.* **2004**, *22*, 198.
[4] X. Michalet, F. F. Pinaud, L. A. Bentolila, J. M. Tsay, S. Doose, J. J. Li, G. Sundaresan, A. M. Wu, S. S. Gambhir, S. Weiss, *Science* **2005**, *307*, 538.
[5] C. Bouzigues, M. Morel, A. Triller, M. Dahan, *Proc. Natl. Acad. Sci. USA* **2007**, *104*, 11251.
[6] M. Howarth, K. Takao, Y. Hayashi, A. Y. Ting, *Proc. Natl. Acad. Sci. USA* **2005**, *102*, 7583.
[7] Y. P. Chang, F. Pinaud, J. Antelman, S. Weiss, *J. Biophotonics* **2008**, *1*, 287.
[8] S. Kim, M. G. Bawendi, *J. Am. Chem. Soc.* **2003**, *125*, 14652.
[9] A. P. Alivisatos, W. Gu, C. Larabell, *Annu. Rev. Biomed. Eng.* **2005**, *7*, 55.
[10] F. Pinaud, D. King, H. P. Moore, S. Weiss, *J. Am. Chem. Soc.* **2004**, *126*, 6115.
[11] B. Dubertret, P. Skourides, D. J. Norris, V. Noireaux, A. H. Brivanlou, A. Libchaber, *Science* **2002**, *298*, 1759.
[12] W. Liu, M. Howarth, A. B. Greytak, Y. Zheng, D. G. Nocera, A. Y. Ting, M. G. Bawendi, *J. Am. Chem. Soc.* **2008**, *130*, 1274.
[13] M. J. Murcia, D. E. Minner, G. M. Mustata, K. Ritchie, C. A. Naumann, *J. Am. Chem. Soc.* **2008**, *130*, 15054.
[14] M. Howarth, W. Liu, S. Puthenveetil, Y. Zheng, L. F. Marshall, M. M. Schmidt, K. D. Wittrup, M. G. Bawendi, A. Y. Ting, *Nat. Methods* **2008**, *5*, 397.
[15] S. Lata, M. Gavutis, R. Tampé, J. Piehler, *J. Am. Chem. Soc.* **2006**, *128*, 2365.
[16] V. Roullier, S. Clarke, C. You, F. Pinaud, G. G. Gouzer, D. Schaible, V. Marchi-Artzner, J. Piehler, M. Dahan, *Nano Lett.* **2009**, *9*, 1228.
[17] A. Reichel, D. Schaible, N. Al Furoukh, M. Cohen, G. Schreiber, J. Piehler, *Anal. Chem.* **2007**, *79*, 8590.
[18] A. R. Clapp, I. L. Medintz, J. M. Mauro, B. R. Fisher, M. G. Bawendi, H. Mattoussi, *J. Am. Chem. Soc.* **2004**, *126*, 301.
[19] A. Sergé, N. Bertaux, H. Rigneault, D. Marguet, *Nat. Methods* **2008**, *5*, 687.
[20] M. Howarth, D. J. Chinnapen, K. Gerrow, P. C. Dorrestein, M. R. Grandy, N. L. Kelleher, A. El-Husseini, A. Y. Ting, *Nat. Methods* **2006**, *3*, 267.

  